PROCEEDINGS OF SPIE

SPIEDigitalLibrary.org/conference-proceedings-of-spie

Using the pupil difference probability density to understand OTF

Kevin Liang, Miguel A. Alonso

Kevin Liang, Miguel A. Alonso, "Using the pupil difference probability density to understand OTF," Proc. SPIE 10694, Computational Optics II, 106940P (28 May 2018); doi: 10.1117/12.2316426

SPIE.

Event: SPIE Optical Systems Design, 2018, Frankfurt, Germany

Downloaded From: https://www.spiedigitallibrary.org/conference-proceedings-of-spie on 15 Mar 2019 Terms of Use: https://www.spiedigitallibrary.org/terms-of-use

Using the pupil difference probability density to understand OTF

Kevin Liang[a,b] and Miguel A. Alonso[a,b,c]

[a]The Institute of Optics, University of Rochester, Rochester NY 14627, USA
[b]Center for Freefrom Optics, University of Rochester, Rochester NY 14627, USA
[c]Aix-Marseille Univ., SNRF, Centrale Marseille, Institut Fresnel, UMR 7249, 13397 Marseille Cedex 20, France

ABSTRACT

We present the definition of a new quantity, the pupil difference probability density (PDPD), and describe its use in the study of imaging systems. Formally, the PDPD is defined as the probability density that two random points over the pupil, with given separation, have a given wavefront error difference. Under this definition, the PDPD is the one-dimensional Fourier transform, of the error difference variable, of the OTF. Using the PDPD, we show that it is possible to understand how certain sources of error affect the OTF. Further, given its geometric interpretation, this formalism is useful for finding accurate analytic approximations to the OTF.

Keywords: OTF, mid-spatial frequency, freeform optics, defocus, astigmatism, mathematical methods

1. INTRODUCTION

The OTF of a system, for a given wavenumber $k = 2\pi/\lambda$, is given by:[1]

$$\mathrm{OTF}(k,\boldsymbol{\rho}) = \frac{\iint A(\boldsymbol{q}-\boldsymbol{\rho}/2)e^{\mathrm{i}kW(\boldsymbol{q}-\boldsymbol{\rho}/2)}A(\boldsymbol{q}+\boldsymbol{\rho}/2)e^{-\mathrm{i}kW(\boldsymbol{q}+\boldsymbol{\rho}/2)}\,\mathrm{d}^2q}{\iint A^2(\boldsymbol{q})\,\mathrm{d}^2q}, \tag{1}$$

where $W(\boldsymbol{q})$ is the aberration function at the pupil point $\boldsymbol{q}$ (in dimensionless pupil units), $A(\boldsymbol{q}) \in [0,1]$ is the pupil amplitude function (which is normally binary, although the treatment we present remains valid for an apodized pupil), and $\boldsymbol{\rho}$ is a pupil coordinate displacement. Although it is a popular and useful metric of optical performance, the expression for the OTF is often difficult to calculate explicitly, for even the simplest of aberrations, and its evaluation is typically done numerically. Although computation speeds today typically enable the calculation of the OTF of a system to be done quickly, it side-steps any physical or geometrical intuition to as to why the OTF is degraded by a certain type of error.

By using a new quantity, named the pupil-difference probability density (PDPD), it is possible to conceptually obtain the OTF from a novel viewpoint. The PDPD, denoted by $P(\eta,\boldsymbol{\rho})$, is defined as a probability density for the error ΔW with given pupil displacement $\boldsymbol{\rho}$. That is, for given $\boldsymbol{\rho}$, $P(\eta,\boldsymbol{\rho})\mathrm{d}\eta$ is the fraction of values of $\boldsymbol{q}$ over the overlap region for which the aberration difference $\Delta W(\boldsymbol{q},\boldsymbol{\rho})$ falls within the infinitesimal range $[\eta,\eta+\mathrm{d}\eta]$. This function can be expressed mathematically as

$$P(\eta,\boldsymbol{\rho}) = \frac{\iint_{O(\boldsymbol{\rho})}\delta[\eta-\Delta W(\boldsymbol{q},\boldsymbol{\rho})]\,\mathrm{d}^2q}{a\,\mathrm{OTF}_{\mathrm{perf}}(\boldsymbol{\rho})}, \tag{2}$$

where δ is the Dirac delta distribution and $\mathrm{OTF}_{\mathrm{perf}}(\boldsymbol{\rho}) = \iint_{O(\boldsymbol{\rho})}\mathrm{d}^2q/a$ is the system's optical transfer function in the absence of errors ($W=0$). We can see from this definition that $\int P(\eta,\boldsymbol{\rho})\,\mathrm{d}\eta = 1$, for any $\boldsymbol{\rho}$, in accordance

Further author information: (Send correspondence to Kevin Liang)
Kevin Liang: E-mail: kliang3@ur.rochester.edu

Computational Optics II, edited by Daniel G. Smith, Frank Wyrowski, Andreas Erdmann, Proc. of SPIE
Vol. 10694, 106940P · © 2018 SPIE · CCC code: 0277-786X/18/$18 · doi: 10.1117/12.2316426

Downloaded From: https://www.spiedigitallibrary.org/conference-proceedings-of-spie on 15 Mar 2019
Terms of Use: https://www.spiedigitallibrary.org/terms-of-use

with its interpretations as a probability density function. With Eq. (2), it is possible to show that there is a simple Fourier relation between the OTF and the PDPD. This is given by

$$\mathrm{OTF}(k,\boldsymbol{\rho}) = \mathrm{OTF}_{\mathrm{perf}}(\boldsymbol{\rho})\widetilde{P}(k,\boldsymbol{\rho}), \tag{3}$$

where

$$\widetilde{P}(k,\boldsymbol{\rho}) = \int P(\eta,\boldsymbol{\rho})e^{\mathrm{i}k\eta}\,\mathrm{d}\eta. \tag{4}$$

The corresponding result for the MTF is

$$\mathrm{MTF}(k,\boldsymbol{\rho}) = \mathrm{MTF}_{\mathrm{perf}}(\boldsymbol{\rho})|\widetilde{P}(k,\boldsymbol{\rho})|, \quad \mathrm{MTF}_{\mathrm{perf}}(\boldsymbol{\rho}) = |\mathrm{OTF}_{\mathrm{perf}}(\boldsymbol{\rho})|. \tag{5}$$

Equations (3) and (5) state the first main result of this work: for systems where W can be regarded as independent of wavelength (e.g. reflective systems), the OTF as a function of wavenumber k is simply the Fourier transform of the PDPD times the OTF of the unaberrated system. Note that for systems in which W does depend on wavelength, this formulation is still valid, i.e., Eq. (4) still applies. However, because $P(\eta,\boldsymbol{\rho})$ then also depends on k, the inverse process of recovering the PDPD from the OTF by inverse Fourier transformation is not possible.

In this work, we focus on two types of error for which the PDPD allows finding simple estimates. The first concerns quadratic errors at the pupil. In this case, the PDPD turns out to have a nice interpretation: it is a projection of the overlap region of two shifted copies of the pupil. Furthermore, an analytic closed form approximation for the OTF can be found by fitting the PDPD with a few function shapes with simple Fourier transforms.

The second type of error are the groove structures often left behind by some freeform manufacturing processes. Sub-aperture freeform manufacturing tools leave behind mid-spatial frequency (MSF) errors, whose effect in optical performance are notoriously difficult to characterize.[2–5] For example, for the typical diamond-milling and turning processes, these errors take the form of either parallel or concentric grooves over the optical part. We show how the PDPD formalism also leads to simple yet accurate analytic estimates.

2. QUADRATIC ERRORS

Previous efforts to find analytic expressions for quadratic errors start with the work by Hopkins[6] and De,[7] who derived infinite series expressions for the OTF of systems with defocus and astigmatism, respectively. Stokseth[8] derived an empirical approximation to Hopkins' result, and FitzGerrel *et al.*[9] proposed a visualization of the effect of defocus on the OTF through the ambiguity function. The approach presented here, on the other hand, allows deriving a simple analytic approximation for the OTF for defocus, whose error is not more than about 1% regardless of the level of aberration.[10] We then extend this result for the OTF to general anisotropic quadratic surface errors, including astigmatism.

2.1 Defocus

We begin with the simplest nontrivial aberration, defocus, given by

$$W_{\mathrm{d}}(\boldsymbol{q}) = h\frac{|\boldsymbol{q}|^2}{R^2}, \tag{6}$$

where h is the amplitude of the error. The error difference is easily found to be a linear function of the pupil coordinate:

$$\Delta W_{\mathrm{d}}(\boldsymbol{q},\boldsymbol{\rho}) = 2h\frac{\boldsymbol{q}\cdot\boldsymbol{\rho}}{R^2}. \tag{7}$$

Given the rotational symmetry, the PDPD and OTF depend only on the magnitude of $\boldsymbol{\rho}$ and not on its direction. It is then sufficient to consider the case in which $\boldsymbol{\rho}$ is in the horizontal direction, so that x and y represent

Downloaded From: https://www.spiedigitallibrary.org/conference-proceedings-of-spie on 15 Mar 2019
Terms of Use: https://www.spiedigitallibrary.org/terms-of-use

respectively the components of $\boldsymbol{q}$ that are parallel and perpendicular to $\boldsymbol{\rho}$. These coordinates are constrained to the intervals $x \in [-x_{\max}, x_{\max}]$, where $x_{\max} = R - \rho/2$, and $y \in [-\mathcal{O}(x,\rho), \mathcal{O}(x,\rho)]$, where

$$\mathcal{O}(x,\rho) = \sqrt{R^2 - \left[|x| + \frac{\rho}{2}\right]^2}\,\mathrm{rect}\left(\frac{x}{2x_{\max}}\right). \tag{8}$$

Note that $2\mathcal{O}(x,\rho)$ is the projection of the overlap region onto the x axis.

From Eq. (7) and Fig. 1(a) we see that the contours of constant ΔW are uniformly-spaced straight lines perpendicular to $\boldsymbol{\rho}$ and so the PDPD, as a function of $\eta = \Delta W$, is simply proportional to the length of these contours. That is, the PDPD for defocus is a scaled version of the projection of the overlap region,

$$P_{\mathrm{d}}(\eta,\rho) = \frac{R^2}{h\rho A_{\mathrm{overlap}}(\rho)}\mathcal{O}\left(\frac{R^2}{2h\rho}\eta,\rho\right), \tag{9}$$

where the change of variables $x \to R^2\eta/(2h\rho)$ guarantees that the range in η over which the PDPD differs from zero coincides with the range of values that ΔW takes within the overlap region, while the prefactor guarantees normalization.

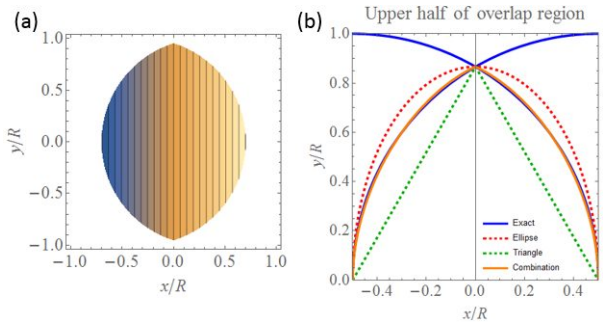

Figure 1. (a) Overlap region and contours of constant ΔW. (b) Exact upper half overlap region (blue), and its approximation (orange) constructed as a linear combination of a half ellipse (red, dashed) and a triangle (green, dashed).

Unfortunately, there is no simple closed-form Fourier transform for the PDPD in Eq. (9), despite its relative simplicity. Nevertheless, it turns out that a surprisingly accurate estimate can be constructed as superposition of two functions with simple Fourier transforms: a half ellipse and a triangle, whose Fourier transforms are, respectively, a Bessel function and a sinc function squared. The equations of these half-ellipse and triangle functions are

$$E(x,\rho) = \frac{\mathcal{O}(0,\rho)}{x_{\max}}\mathrm{Re}\left[\sqrt{x_{\max}^2 - x^2}\right], \tag{10a}$$

and

$$T(x,\rho) = \mathcal{O}(0,\rho)\,\mathrm{triangle}\left(\frac{x}{x_{\max}}\right), \tag{10b}$$

respectively, where $\mathrm{triangle}(x)$ is the unit triangle function. The total approximation to $\mathcal{O}(x,\rho)$, denoted by $\mathcal{O}_{\mathrm{a}}(x,\rho)$, is given by a superposition that matches the exact result at $x = 0$, namely

$$\mathcal{O}_{\mathrm{a}}(x,\rho) = w(\rho)E(x,\rho) + [1 - w(\rho)]T(x,\rho), \tag{11}$$

where the weight factor $w(\rho)$ is chosen so that the area of $\mathcal{O}_{\mathrm{a}}$ matches that of $\mathcal{O}$.[10] The corresponding approximate expression for the OTF is

$$\mathrm{OTF}_{\mathrm{d}}(k,\rho) \approx \frac{\mathcal{O}_{\mathrm{a}}(0,\rho)}{h\rho}\left[\frac{w}{k}J_1(k\eta_0) + \frac{\eta_0(1-w)}{\pi}\,\mathrm{sinc}^2\left(\frac{k\eta_0}{2}\right)\right], \tag{12}$$

where $\eta_0 = 2h\rho x_{\max}/R^2$. Figure 2 compares this result with numerically calculated OTF values.

Downloaded From: https://www.spiedigitallibrary.org/conference-proceedings-of-spie on 15 Mar 2019
Terms of Use: https://www.spiedigitallibrary.org/terms-of-use

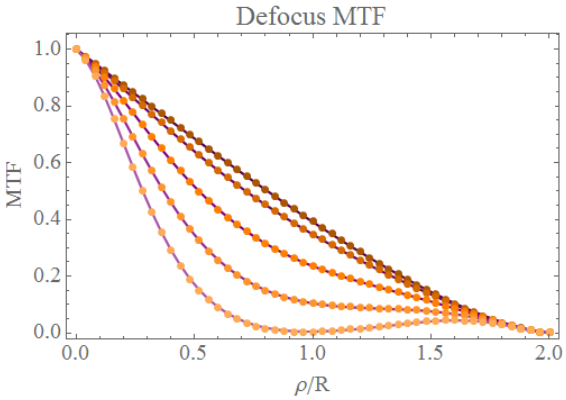

Figure 2. Approximate MTF (magnitude of the OTF) in Eq. (12) (solid), along with numerically calculated values (orange dots), for kh varying from 0 (darkest) to 4 (brightest) in steps of 1.

2.2 Anisotropic quadratic errors

It is possible to extend these results to general quadratic surface errors given by the expression

$$W_{\text{quad}}(x, y) = \frac{ax^2 + by^2 + 2cxy}{2R^2}, \tag{13}$$

where a, b, and c are amplitude coefficients. Given the anisotropy of W_{quad} the PDPD and OTF now depend on both the magnitude and direction of $\boldsymbol{\rho}$. The error difference, however, is still a linear function of the pupil position:

$$\Delta W_{\text{quad}}(x, y, \boldsymbol{\rho}) = \frac{(a\rho_x + c\rho_y)x + (b\rho_y + c\rho_x)y}{R^2}. \tag{14}$$

That is, as shown in Fig. 3, the contours of constant ΔW_{quad} are again uniformly-spaced straight lines, but these are no longer perpendicular to the pupil displacement. It is then convenient to introduce a rotated coordinate system (x', y'), also shown in Fig. 3, determined by an angle of rotation $\theta(\boldsymbol{\rho})$. In this system, ΔW_{quad} depends on only the coordinate x':

$$\Delta W_{\text{quad}}(x', \boldsymbol{\rho}) = -x' C_{\text{quad}}(\boldsymbol{\rho}), \tag{15}$$

where

$$C_{\text{quad}}(\boldsymbol{\rho}) = \frac{\sqrt{(a^2 + c^2)\rho_x^2 + 2(a + b)c\rho_x\rho_y + (b^2 + c^2)\rho_y^2}}{R^2}. \tag{16}$$

We arrive at the result for the PDPD of a general quadratic surface error:

$$P_{\text{quad}}(\eta, \boldsymbol{\rho}) = \frac{\mathfrak{T}[\widehat{\eta}(\eta, \boldsymbol{\rho}), \boldsymbol{\rho}]}{C_{\text{quad}}(\boldsymbol{\rho}) A_{\text{overlap}}(\rho)}, \tag{17}$$

where $\mathfrak{T}(x', \boldsymbol{\rho})$ is the projection of the overlap region onto the x' axis, and $\widehat{\eta}(\eta, \boldsymbol{\rho}) = \eta / C_{\text{quad}}(\boldsymbol{\rho})$. Note that this expression holds for any pupil shape, since this shape is only reflected on the functional form of $\mathfrak{T}$. For a circular pupil, $\mathfrak{T}(x', \boldsymbol{\rho})$ is given by

$$\mathfrak{T}(x', \boldsymbol{\rho}) = \begin{cases} \mathfrak{T}_1(x', \boldsymbol{\rho}), & x \in [-x'_{\text{M}}, -x'_{\text{c}}], \\ \mathfrak{T}_2(x', \boldsymbol{\rho}), & x \in [-x'_{\text{c}}, x'_{\text{c}}], \\ \mathfrak{T}_3(x', \boldsymbol{\rho}), & x \in [x'_{\text{c}}, x'_{\text{M}}], \\ 0, & \text{otherwise}, \end{cases} \tag{18}$$

Downloaded From: https://www.spiedigitallibrary.org/conference-proceedings-of-spie on 15 Mar 2019
Terms of Use: https://www.spiedigitallibrary.org/terms-of-use

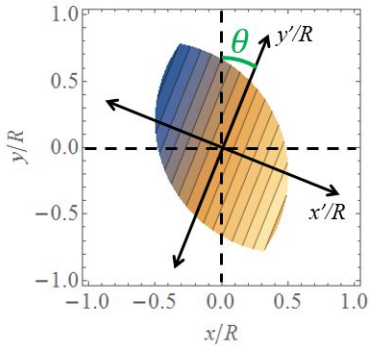

Figure 3. Here, ΔW_{quad} is shown for $a = -b, c = 0$ in the overlap region. By rotating (x, y) by θ, gives a new coordinate system (x', y') where the contours are vertical.

where the functions $\mathfrak{T}_i(x', \boldsymbol{\rho})$ are given by

$$\mathfrak{T}_1(x') = 2\mathfrak{C}_-(x', \rho'_x), \tag{19a}$$
$$\mathfrak{T}_2(x') = \mathfrak{C}_+(x', \rho'_x) + \mathfrak{C}_-(x', \rho'_x) - |\rho'_y|, \tag{19b}$$
$$\mathfrak{T}_3(x') = 2\mathfrak{C}_+(x', \rho'_x), \tag{19c}$$

with $\mathfrak{C}_\pm(x', \rho'_x) = \sqrt{R^2 - (x' \pm |\rho'_x|/2)^2}$. The limits of the ranges in Eq. (18) are the x' coordinates of the overlap region's cusps, $\pm x'_{\text{c}}$, and the location of the overlap region's minimum and maximum x' values, $\pm x'_{\text{M}}$.

Notice from Eq. (18) that there are three cases to consider, illustrated in Fig. 4. For the first case, shown in (a), none of the regions have empty domains and $\mathfrak{T}$ is composed of three nonzero segments. The second case, shown in (b), corresponds to $x'_{\text{c}} = 0$, for which $\mathfrak{T}_3(x', \boldsymbol{\rho})$ has an empty domain (as in the case of defocus). The third case, shown in (c), corresponds to $x'_{\text{M}} = x'_{\text{c}}$, for which both $\mathfrak{T}_1(x', \boldsymbol{\rho})$ and $\mathfrak{T}_3(x', \boldsymbol{\rho})$ have empty domains so that $\mathfrak{T}_3(x', \boldsymbol{\rho})$ is the only non-zero region.

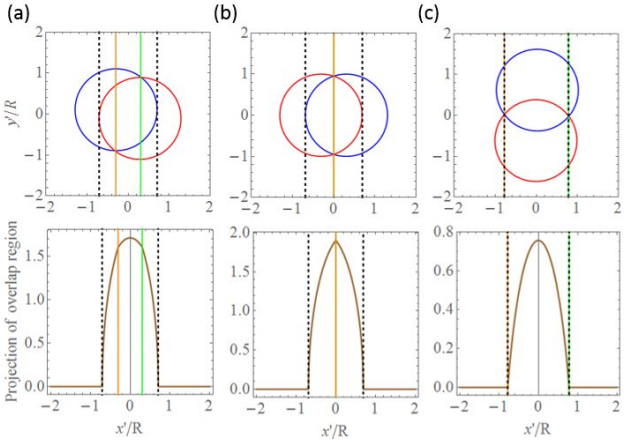

Figure 4. Projections of the overlap regions for the cases when (a) $0 \neq x'_{\text{c}} \neq x'_{\text{M}}$, (b) $x'_{\text{c}} = 0$, and (c) $x'_{\text{c}} = x'_{\text{M}}$. The green and orange lines indicate the locations of $\pm x'_{\text{c}}$, respectively, and the black dashed lines indicate the locations of $\pm x'_{\text{M}}$.

As in the case of defocus, Eq. (17) provides a geometric link between the PDPD of quadratic errors and the projection of the pupils' overlap area, but the result does not admit a simple closed-form Fourier transform to obtain the OTF. To address this issue, we again propose an approximation to the PDPD in terms of simple functions with simple Fourier transforms. The proposed approximation to the overlap region is given by

$$\Phi(x', \boldsymbol{\rho}) = w_E(\boldsymbol{\rho})E(x', \boldsymbol{\rho}) + w_D(\boldsymbol{\rho})D(x', \boldsymbol{\rho}) + w_T(\boldsymbol{\rho})T(x', \boldsymbol{\rho}), \tag{20}$$

Downloaded From: https://www.spiedigitallibrary.org/conference-proceedings-of-spie on 15 Mar 2019
Terms of Use: https://www.spiedigitallibrary.org/terms-of-use

for $|x'| \le x'_{\mathrm{M}}$ and zero otherwise, where the basic functions are a half ellipse, a parabolic segment, and a trapezium (the difference of two similar triangles):

$$E(x',\boldsymbol{\rho}) = \frac{M(\boldsymbol{\rho})}{x'_{\mathrm{M}}}\sqrt{x'^2_{\mathrm{M}} - x'^2}, \tag{21a}$$

$$D(x',\boldsymbol{\rho}) = \frac{M(\boldsymbol{\rho})}{x'^2_{\mathrm{M}}}(x'^2_{\mathrm{M}} - x'^2), \tag{21b}$$

$$T(x',\boldsymbol{\rho}) = \frac{Q(\boldsymbol{\rho})}{x'_{\mathrm{M}} - x'_{\mathrm{c}}}\left[x'_{\mathrm{M}}\mathrm{triangle}\left(\frac{x'}{x'_{\mathrm{M}}}\right) - x'_{\mathrm{c}}\mathrm{triangle}\left(\frac{x'}{x'_{\mathrm{c}}}\right)\right]. \tag{21c}$$

Furthermore, $Q(\boldsymbol{\rho}) = \mathfrak{T}_3(x'_{\mathrm{c}},\boldsymbol{\rho})$ is the value of $\mathfrak{T}$ at the cusps, and $M(\boldsymbol{\rho}) = \mathfrak{T}_2(0,\boldsymbol{\rho})$ is the maximum value of $\mathfrak{T}$. The weights are chosen to preserve the area of the overlap region.[10] Notice that in the limit when the aberration is rotationally symmetric (defocus), the parabola disappears and the trapezium reduces to a triangle, recovering the previous result.

By using this approximation, the PDPD can be estimated as

$$P_{\mathrm{quad}}(\eta,\boldsymbol{\rho}) \approx \frac{\Phi[\widehat{\eta}(\eta,\boldsymbol{\rho}),\boldsymbol{\rho}]}{C_{\mathrm{quad}}(\boldsymbol{\rho})A_{\mathrm{overlap}}(\rho)}, \tag{22}$$

and its Fourier transform gives the following approximate OTF:

$$\begin{aligned}\mathrm{OTF}_{\mathrm{quad}}(k,\boldsymbol{\rho}) \approx \frac{1}{C_{\mathrm{quad}}(\boldsymbol{\rho})R^2}\Bigg\{ & w_E(\boldsymbol{\rho})M(\boldsymbol{\rho})\frac{J_1(k\eta_{\mathrm{M}})}{k} \\ & + \frac{4w_D(\boldsymbol{\rho})M(\boldsymbol{\rho})}{\pi\eta_{\mathrm{M}}^2}\left[\frac{\sin(k\eta_{\mathrm{M}}) - \eta_{\mathrm{M}}k\cos(k\eta_{\mathrm{M}})}{k^3}\right] \\ & + \frac{2w_T(\boldsymbol{\rho})Q(\boldsymbol{\rho})}{\pi(\eta_{\mathrm{M}} - \eta_{\mathrm{c}})}\left[\frac{\cos(k\eta_{\mathrm{c}}) - \cos(k\eta_{\mathrm{M}})}{k^2}\right]\Bigg\},\end{aligned} \tag{23}$$

where $\eta_{\mathrm{M}} = C_{\mathrm{quad}}(\boldsymbol{\rho})x'_{\mathrm{M}}$ and $\eta_{\mathrm{c}} = C_{\mathrm{quad}}(\boldsymbol{\rho})x'_{\mathrm{c}}$. A comparison of the MTFs calculated from Eq. (23) with those computed numerically is seen in Fig. (5). The RMS error is around 1%.

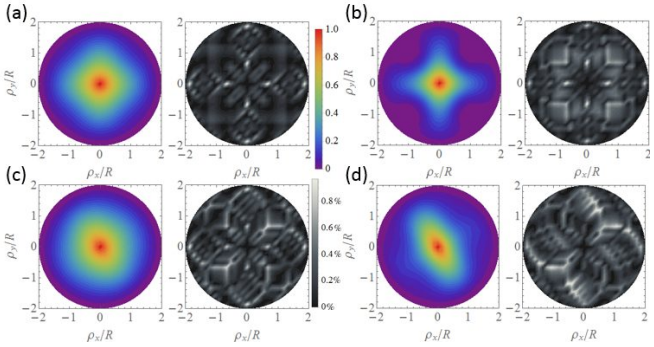

Figure 5. Numerically generated MTF (colored left plots) and percentage difference between the numerical MTFs and the analytic forms in Eq. (23) (grayscale right plots), for (ka, kb, kc) equal to: $(2,-2,0)$ (a), $(4,-4,0)$ (b), $(2,2/3,1)$ (c), and $(4,4/3,2)$ (d). The maximum difference is less than 1%.

3. PERIODIC ERRORS

Freeform manufacturing tools, which are typically smaller than the optical surface they are finishing/polishing, leave behind errors whose characteristic frequencies are between those described by low-order Zernike terms and those attributed to surface roughness. These errors, known as mid-spatial frequency (MSF) errors, pose a range

Downloaded From: https://www.spiedigitallibrary.org/conference-proceedings-of-spie on 15 Mar 2019
Terms of Use: https://www.spiedigitallibrary.org/terms-of-use

of performance issues.[2–5] Especially important for manufacturers, they complicate the ability to set effective tolerances for surface quality.

As mentioned in Sec. 1, the PDPD can be used to understand how periodic errors affect the OTF.[11] Similar methods were shown to be effective on another metric of optical performance: the Strehl ratio.[12] In fact, the methods presented here is valid for errors that are periodic with any frequency, not just those of MSF.

3.1 One-dimensional examples

To illustrate how the PDPD gives a simple picture of MTF performance, we now consider four different periodic error patterns in one dimension: a binary rectangular groove with fill factor 1/2, a symmetric triangular groove, a sinusoidal groove, and a piecewise parabolic groove. These groove profiles are chosen because their simplicity helps illustrate the concepts introduced here and allow analytic solutions. In particular, the piecewise parabolic groove structure mimics the profile left behind by a diamond tool. For all patterns, the spatial period is denoted by T and the peak-to-valley height by h. Throughout, the dependence on the one-dimensional separation ρ is expressed in terms of the shorthands $\widehat{\rho}_T = (\rho \bmod T)/T$ and $z = 1 - |1 - 2\widehat{\rho}_T|$. The groove patterns we examine, and the corresponding PDPD and its Fourier transform are presented in Table 1. Illustrations of these results is shown in Fig. 6. The plots for the PDPD within the second column are shown on their side so that they can be related to the error differences shown in purple in the first column.

Table 1. Four groove shapes with their PDPD (second column) and the PDPD Fourier transform (third column).

Groove shape	$P(\eta, \rho)$	$\widetilde{P}(k, \rho)$
 Rectangular	$\frac{z}{2}\left[\delta(\eta - h) + \delta(\eta + h)\right]$ $+(1-z)\delta(\eta)$	$z\cos(kh)$ $+(1-z)$
 Triangular	$\frac{1-z}{2}\left[\delta(\eta - zh) + \delta(\eta + zh)\right]$ $+\frac{1}{2h}\mathrm{rect}\left(\frac{\eta}{2zh}\right)$	$(1-z)\cos(zkh)$ $+\frac{\sin(zkh)}{kh}$
 Sinusoidal	$\mathrm{Re}\left(\frac{1}{\pi\sqrt{[h\sin(\pi\widehat{\rho}_T)]^2 - \eta^2}}\right)$	$J_0[kh\sin(\pi\widehat{\rho}_T)]$
 Piecewise parabolic	$\frac{1}{8h\widehat{\rho}_T(1-\widehat{\rho}_T)}\mathrm{rect}\left[\frac{\eta}{8h\widehat{\rho}_T(1-\widehat{\rho}_T)}\right]$	$\frac{\sin[4kh\widehat{\rho}_T(1-\widehat{\rho}_T)]}{4kh\widehat{\rho}_T(1-\widehat{\rho}_T)}$

Downloaded From: https://www.spiedigitallibrary.org/conference-proceedings-of-spie on 15 Mar 2019
Terms of Use: https://www.spiedigitallibrary.org/terms-of-use

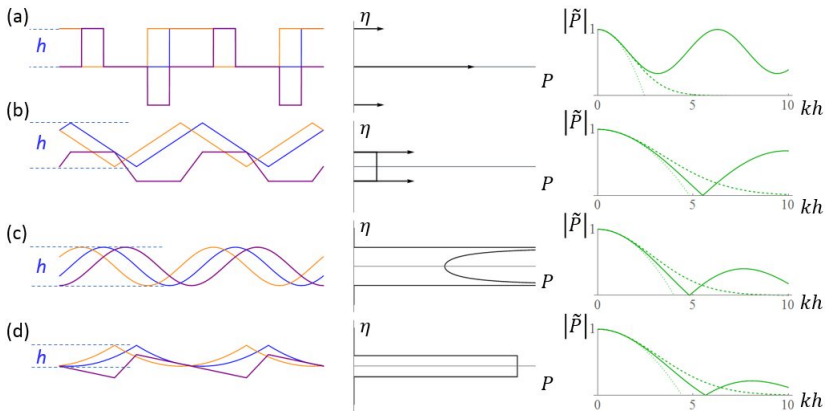

Figure 6. The PDPD functions for one-dimensional (a) rectangular, (b) triangular, (c) sinusoidal, and (d) piecewise parabolic periodic groove patterns. The left column shows two copies of the groove pattern (blue and orange) separated by ρ, and their difference (purple). The center and right columns are the corresponding PDPD and the modulus its Fourier transform (solid green). The dashed and dotted green lines show the approximations $1-k^2D(\rho)^2/2$ and $\exp[-k^2D(\rho)^2/2]$, described in Section 6. Here, we used $\rho = T/6$.

3.2 Parallel groove patterns

Here we show how the PDPD can be used to understand typical groove structures left behind by diamond milling: parallel tracks as seen in Fig. 7(a). If the surface in question is located near a plane conjugate to the aperture stop, the error W at the pupil is approximately proportional to the surface error. Consider, for example, a circular pupil of radius R across which the error has the shape of grooves aligned with the y-axis. Under the assumption that R is much larger than the groove width T we can use the approximation $P(\eta, \boldsymbol{\rho}) \approx P_1(\eta, \rho_x)$, where ρ_x is the x-component of $\boldsymbol{\rho}$. This means that the MTF is given by

$$\mathrm{MTF}(k, \boldsymbol{\rho}) \approx \mathrm{MTF}_{\mathrm{perf}}(\boldsymbol{\rho}) |\widetilde{P}_1(k, \rho_x)|. \tag{24}$$

Figure 7 illustrates this result for the case of 5 parabolic groove profiles across the pupil.

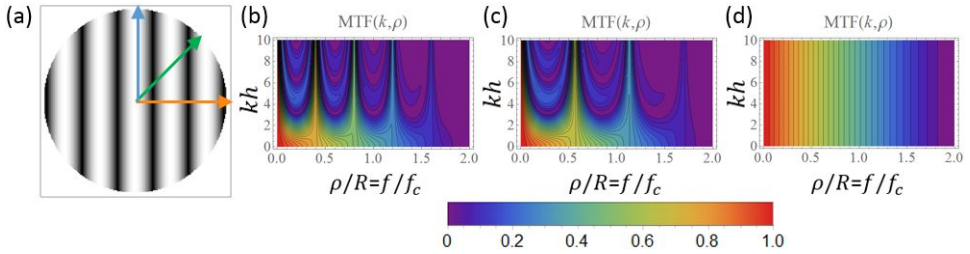

Figure 7. (a) Circular pupil whose error presents five parabolic grooves of height h across its diameter, aligned in the vertical direction. (b-d) MTF as a function of both kh and spatial frequency for different radial slices, corresponding to the directions of the orange, green, and blue arrows shown in (a). The axis variable ρ/R equals the normalized spatial frequency f/f_c, where f is the spatial frequency in the direction of the radial slice and f_c is the coherent cutoff frequency for the circular pupil.

3.3 Concentric groove patterns

The framework of the PDPD shows its true power when applied to a system for which the errors are composed of concentric circular grooves with identical cross sections. These are the typical types of groove tracks left behind by diamond turning. This means, in this case, the error is only a function of the radial pupil coordinate q with radial period T. It is the rotational symmetry of such a problem that can be explicitly exploited in ways that would otherwise be difficult to do without the PDPD. The PDPD is shown to be be expressed as:[11]

$$P(\eta, \rho) \approx \frac{1}{F(\rho)} \left[\frac{A(\rho)}{2} \hat{\mathcal{Q}}_t P_1(\eta, \rho) + \frac{B(\rho)}{\sqrt{2}} \hat{\mathcal{Q}}_\tau \overline{P}_1(\eta, \rho/2) + E(\rho) P_0(\eta) \right], \tag{25}$$

Downloaded From: https://www.spiedigitallibrary.org/conference-proceedings-of-spie on 15 Mar 2019
Terms of Use: https://www.spiedigitallibrary.org/terms-of-use

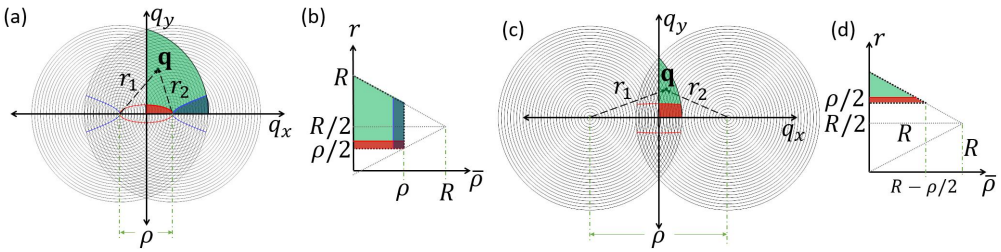

Figure 8. Diagrams representing the various coordinates, for $\rho < R$ (a,b) and $\rho \geq R$ (c,d). In (a) and (c), two copies of the pupil with a rotationally symmetric periodic groove pattern are shown, mutually displaced by ρ. The distances to a given point $\mathbf{q}$ from the centers of the pupils are r_1 and r_2. The elliptic and hyperbolic (red and blue) regions in the (q_x, q_y) space over which both sets of grooves are nearly parallel map onto straight bands (red and blue) in the $(\overline{\rho}, r)$ space.

and the corresponding OTF estimate is found as $4F$ times the Fourier transform in η of this result:

$$\mathrm{OTF}(k,\rho) \approx 4\left[\frac{A(\rho)}{2}\hat{\mathcal{Q}}_t\widetilde{P}_1(k,\rho) + \frac{B(\rho)}{\sqrt{2}}\hat{\mathcal{Q}}_\tau\widetilde{\overline{P}}_1(k,\rho/2) + E(\rho)\widetilde{P}_0(k)\right]. \tag{26}$$

In these results, $A(\rho), B(\rho)$, and $E(\rho)$ are the areas shown in blue, red, and green in Fig. 8, respectively, such that $A(\rho) + B(\rho) + E(\rho) = F(\rho)$. Note that if the pupil were noncircular or if it were not centered at the center of the grooves (due, for example, to an off-axis beam footprint), the approximate result above would still be valid, as long as the areas A, B, E, and F are calculated with the appropriate boundaries. Furthermore, the quantities associated to $P_1, \overline{P}_1$, and P_0 are directly related to the one-dimensional PDPD that corresponds to the groove profile of the tracks. This directly links the one-dimensional results to this case. Also, $t = \mathrm{Min}(\rho, T)$ and $\tau = -\mathrm{Min}(2R - \rho, T)$, and the integral operator $\hat{\mathcal{Q}}_x$ applied to a function $f(\rho)$ is defined as

$$\hat{\mathcal{Q}}_x f(\rho) = \int_0^1 \frac{f(\rho - xv)}{\sqrt{v}}\,\mathrm{d}v. \tag{27}$$

Since this operator has the form of a convolution and is applied to periodic functions with period T, the easiest way to calculate its effect is through a Fourier series expansion of the function it acts on. That is, if the periodic function (assumed here to be even) is written as

$$f(\rho) = \frac{1}{2}a_0 + \sum_{m=1}^{\infty} a_m \cos\left(\frac{2\pi m\rho}{T}\right), \tag{28}$$

then it can be shown that this operator simply modifies the Fourier series as

$$\begin{aligned}\hat{\mathcal{Q}}_x f(\rho) = {} & a_0 \\ & + \sqrt{\frac{T}{|x|}}\sum_{m=1}^{\infty}\frac{a_m}{\sqrt{m}}\left[C\left(2\sqrt{\frac{m|x|}{T}}\right)\cos\left(\frac{2\pi m\rho}{T}\right) + \mathrm{sgn}(x)S\left(2\sqrt{\frac{m|x|}{T}}\right)\sin\left(\frac{2\pi m\rho}{T}\right)\right],\end{aligned} \tag{29}$$

where C and S are the Fresnel cosine and sine integrals, respectively. Hence, in order to solve the integrals in Eq. (26), we have to find the Fourier coefficients a_m for $\widetilde{P}_1$. These coefficients are summarized in Table 2 for the 1D PDPD Fourier transforms in Table 1. Note that, for computational purposes, only a finite number of terms in the Fourier series are used, and the number required to achieve a given level of error depends on kh. The last column on Table 2, labelled as $m_{10\%}$, gives a simple estimate of the terms $m \leq \mathrm{Max}(0, m_{10\%})$ to be used to achieve an error of under 10%. In all cases, a single Fourier coefficient ($m = 1$) is sufficient to achieve this level of error for peak-to-valley aberration heights up to about half a wavelength. Finally, notice that $\widetilde{P}_0(k)$ in Eq. (26) corresponds simply to $a_0/2$, given explicitly in Table 2.

Downloaded From: https://www.spiedigitallibrary.org/conference-proceedings-of-spie on 15 Mar 2019
Terms of Use: https://www.spiedigitallibrary.org/terms-of-use

Table 2. Fourier expansion coefficients (second and third columns) for the functions $\widetilde{P}(k,\rho)$ in Table 1, corresponding to the groove structures shown in the first column. The fourth column shows an estimate of how many Fourier terms are needed ($m \leq \mathrm{Max}(0, m_{10\%})$) for the truncated Fourier series to achieve an error below 10%.

Groove shape	$\widetilde{P}_0(k) = a_0/2$	a_m	$m_{10\%}$
 Rectangular	$\dfrac{1+\cos(kh)}{2}$	$[1-\cos(kh)]\dfrac{2[1-(-1)^m]}{m^2\pi^2}$	1
 Triangular	$\dfrac{2-2\cos(kh)}{k^2h^2}$	$\dfrac{4k^2h^2[1-(-1)^m\cos(kh)]}{(k^2h^2-m^2\pi^2)^2}$	-0.375 $+0.330kh$
 Sinusoidal	$J_0^2(kh/2)$	$2J_m^2(kh/2)$	-0.851 $+0.481kh$
 Piecewise parabolic	$\dfrac{\pi}{2kh}\left[C^2\left(\sqrt{\dfrac{2kh}{\pi}}\right)+S^2\left(\sqrt{\dfrac{2kh}{\pi}}\right)\right]$	$\dfrac{\pi}{8\lvert kh\rvert}\left\lvert \mathrm{Erfi}\left[\dfrac{(1+\mathrm{i})(2kh-m\pi)}{4\sqrt{kh/2}}\right]+\mathrm{Erfi}\left[\dfrac{(1+\mathrm{i})(2kh+m\pi)}{4\sqrt{kh/2}}\right]\right\rvert^2$	-1.184 $+0.521kh$

Figure 9 shows plots of these MTF estimates for the same four groove patterns, as well as of each of the three individual contributions to the estimate in Eq. (26), for $kh = 1.6$. Notice that for $kh \neq 0$ the MTF presents an initial peak for $\rho < T$, followed by oscillations around a baseline, shown in gray in Fig. 9; this general behavior for the MTF has been described before by employing a different approach.[2] It turns out that the equation for this baseline is very simple, and gives a basic estimate of the MTF for $\rho > T$. Note from Eq. (29) and the fact that $a_0 = 2\widetilde{P}_0(k)$ that the first and second terms in Eq. (26) include parts proportional to $\widetilde{P}_0(k)$, and that these, added to the third term of Eq. (26), give simply $\mathrm{MTF}_{\mathrm{perf}}(\rho)\widetilde{P}_0(k)$. Therefore, this baseline is simply the MTF of the unaberrated system scaled by $\widetilde{P}_0(k)$. The number of oscillations around the baseline is precisely the number of periods across the surface. The amplitude of these oscillations depend on both the number of periods across the surface, from the OTF's dependence on $A(\rho)$ and $B(\rho)$, and h from the OTF's dependence on the Fourier coefficients a_m, shown in Table 2.

4. CONCATENATION OF ERRORS

There are often multiple error contributions within a single optical system, which may come from separate surfaces, different manufacturing processes for a single surface, or fluctuating media such as the atmosphere. If these errors are approximately uncorrelated, the total PDPD is constructed following the standard concatenation rule for independent probability densities, as a convolution of the PDPDs P_i from each contribution:

$$P(\eta, \boldsymbol{\rho}) = (P_1 * P_2 * \cdots * P_n)(\eta, \boldsymbol{\rho}). \tag{30}$$

Downloaded From: https://www.spiedigitallibrary.org/conference-proceedings-of-spie on 15 Mar 2019
Terms of Use: https://www.spiedigitallibrary.org/terms-of-use

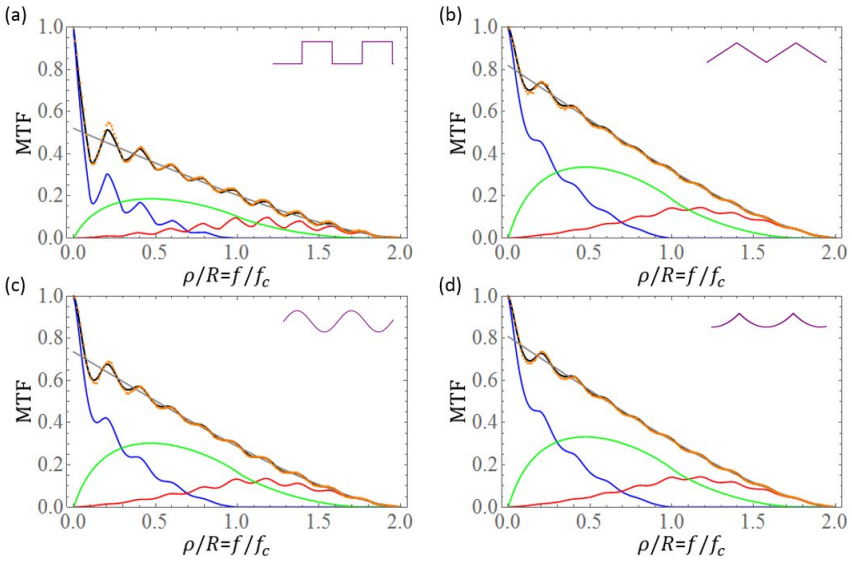

Figure 9. MTF for the four simple circular groove shapes, for $kh = 1.6$. In each figure, the orange dots correspond to a numerical computation, of the MTF, the black curve corresponds to the estimate in Eq. (26), and the blue, red and green curves correspond to the contributions from each of the terms in Eq. (26), in that order. The gray curves show the baseline $\mathrm{MTF}_{\mathrm{perf}}(\rho)\widetilde{P}_0(k)$.

Then, from the Fourier convolution theorem, the MTF of the total system is simply the MTF of the unaberrated system times the product of the Fourier transforms of the individual PDPDs:[13]

$$\mathrm{MTF}(k,\boldsymbol{\rho}) = \mathrm{MTF}_{\mathrm{perf}}(\boldsymbol{\rho}) \prod_{i=1}^{n} |\widetilde{P}_i(k,\boldsymbol{\rho})|. \tag{31}$$

Note that, for this relation to hold, the two different error contributions do not need to be uncorrelated due to independent random fluctuations, but simply from the point of view of the PDPD; for example, two deterministic groove structures in different directions or with different periods have PDPDs that are effectively uncorrelated. This is because, for any given $\boldsymbol{\rho}$, if we were to pick a large series of points $\mathbf{q}$ spanning the overlap region, the values of ΔW for the two contributions would be largely uncorrelated.

It can also be shown that the PDPD is related to another error measure that has been used to study effects on optical performance: the structure function.[14–16] It turns out that the PDPD is more general than the structure function as the structure function $D(\boldsymbol{\rho})$ is just the variance of the PDPD:

$$D(\boldsymbol{\rho}) = \iint_{O(\boldsymbol{\rho})} \Delta W^2(\boldsymbol{q},\boldsymbol{\rho})\, \mathrm{d}^2 q = \int \eta^2 P(\eta,\boldsymbol{\rho})\, \mathrm{d}\eta. \tag{32}$$

Furthermore, the PDPD lends itself, as a probability density function, to the incorporation of more realistic errors. For example, realistic groove tracks left behind by manufacturing tools, or the sinusoidal thermal cycling seen in freeform manufacturing, may not be perfectly periodic. There can be randomness introduced in both the amplitude and periodicity of these errors. Since the PDPD itself is a probabilistic quantity, it can easily be incorporated easily with the random variables that govern the fluctuations in amplitude and period of more realistic errors.

5. CONCLUDING REMARKS

The PDPD has been shown to be insightful in understanding the effects of MSF errors on optical performance. Specifically, the processes of diamond milling and turning were studied, but the theory was demonstrated for various groove profiles and so the results for this project could be extended to other types of MSF contributions, such as thermal cycling. The theme of the PDPD is its ability to exploit geometries that would otherwise

Downloaded From: https://www.spiedigitallibrary.org/conference-proceedings-of-spie on 15 Mar 2019
Terms of Use: https://www.spiedigitallibrary.org/terms-of-use

be difficult to use in the OTF domain. Furthermore, we saw how the PDPD can be used to understand the concatenation of uncorrelated errors within an optical system. As mentioned earlier, the PDPD also provides a foundation to tackle more realistic problems where quasi-periodic errors are present through its interpretation as a probability density.

Going beyond MSF structures, the PDPD can also be used to understand quadratic surface errors - including those of defocus and astigmatism. An elegant geometric property of projections was revealed when the PDPD was implemented, showing that the PDPD is just a projection of the overlap region (an idea that can be extended to non-circular binary apertures). Once this geometry was understood, it was possible to approximate these projections with shapes with well-known Fourier transforms in order to get closed-form expressions for the OTF that are accurate to within 1%.

ACKNOWLEDGMENTS

We thank the members of CeFO for their support and insights, and acknowledge in particular useful discussions with Thomas Suleski, Reza Aryan, Christoph Menke, Thomas Köhler, Flemming Tinker, James Fienup, Angela Davies, Chris Evans, Jannick Rolland, and Greg W. Forbes.

National Science Foundation (NSF) I/UCRC Center for Freeform Optics (IIP-1338877).

REFERENCES

[1] Goodman, J. W., [Introduction to Fourier Optics], Roberts & Company Publishers, Chap. 6 (2005).
[2] Noll, R. J., "Effect of Mid- and High-Spatial Frequencies on Optical Performance," Opt. Eng. **18**(2), 182137 (1979).
[3] Aikens, D., DeGroote, J. E., and Youngworth, R. N., "Specification and Control of Mid-Spatial Frequency Wavefront Errors in Optical Systems," in Frontiers in Optics 2008/Laser Science XXIV/Plasmonics and Metamaterials/Optical Fabrication and Testing, OSA Technical Digest (CD) OSA, paper OTuA1 (2008).
[4] Tamkin, J. M., Milster, T. D., and Dallas, W., "Theory of modulation transfer function artifacts due to mid-spatial-frequency errors and its application to optical tolerancing," Appl. Opt. **49**, 4895-4835 (2010).
[5] Forbes, G. W., "Never-ending struggles with mid-spatial frequencies," Optical Measurement Systems for Industrial Inspection IX, Proc. of SPIE **9525**, 95251B (2015).
[6] Hopkins, H. H., "The frequency response of a defocused optical system," Proc. Roy. Soc. Lond. **A231**, 91-103 (1955).
[7] De, M., "The influence of astigmatism on the response function of an optical system," Proc. Roy. Soc. Lond. **A233**, 91-104 (1995).
[8] Stokseth, P. A., "Properties of a Defocused Optical System," J. Opt. Soc. Am. **59**, 1314-1321 (1969).
[9] FitzGerrell, A. R., Dowski, E. R. Jr., and Cathey, W. T., "Defocus transfer function for circularly symmetric pupils," Appl. Opt. **36**, 5796-5804 (1997).
[10] Liang, K. and Alonso, M. A., "Effects of defocus and other quadratic errors on OTF," Opt. Lett. **42**, 5254-5257 (2017).
[11] Liang, K. and Alonso, M. A., "Understanding the effects of groove structures on the MTF," Opt. Express **25**, 18827-18841 (2017).
[12] Alonso, M. A. and Forbes, G. W., "The Strehl ratio as the Fourier transform of a probability density," Opt. Lett. **41**, 3735-3738 (2016).
[13] Boremann, G. D., "Modulation Transfer Function in Optical and Electro-Optical Systems" SPIE, pp. 85-88 (2001).
[14] He, L., Evans, C. J., and Davis, A., "Two-quadrant area structure function analysis for optical surface characterization," Opt. Express **20**, 23275-23280 (2012).
[15] He, L., Evans, C. J., and Davis, A., "Optical surface characterization with the area structure function," CIRP Annals - Manufacturing Technology, **62**(1), 539-542 (2013).
[16] Parks, R. E. and Tuell, M. T., "The structure function as a metric for roughness and figure," Proc. of SPIE **9951** 99510J-1 (2016).

Downloaded From: https://www.spiedigitallibrary.org/conference-proceedings-of-spie on 15 Mar 2019
Terms of Use: https://www.spiedigitallibrary.org/terms-of-use